Coupled electro-thermal modeling of lithium-ion batteries for electric vehicle application

Tedjani Mesbahi, Rocío Bendala Sugrañes, Reda Bakri, Patrick Bartholomeüs

Coupled Electro-Thermal Modeling of Lithium-ion Batteries For Electric Vehicle Application

Tedjani Mesbahi[a,*], Rocío Bendala Sugrañes[b], Reda Bakri[b], Patrick Bartholomeus[b]

[a] *ICube (UMR CNRS 7357), INSA Strasbourg, FRANCE*
[b] *Univ. Lille, Centrale Lille, Arts et Metiers ParisTech, HEI, HeSam, EA 2697 L2EP - Laboratoire d'Electrotechnique et d'Electronique de Puissance Lille, FRANCE*

Abstract

The lithium-ion battery is a complex system that is both non-linear and non-stationary, which involves electrical, thermal and electrochemical dynamics. In order to deepen the understanding of battery system dynamics, in this paper, an electro-thermal coupled model is proposed for a 40 Ah lithium-ion battery cell with Nickel Manganese Cobalt Oxide cathode material and graphitic anode. The developed model takes into account the dynamics of the high power applications and then allows to accurately present the physicochemical phenomena occurring in a battery cell. It is built through a dynamic equivalent circuit and a thermal model. The battery is divided into n m nodes with two dimensions and each node is represented by an equivalent circuit. Both models are coupled in the same loop, the electric-thermal through the distribution of power losses to calculate the distribution of temperature and the thermal-electric through the mean temperature of the battery to update the electric parameters. The obtained results show that the proposed model is able to simulate the dynamic interaction between the electric and the thermal battery behavior, and high performance for the cell surface temperature prediction.

Keywords: Electro-thermal model, battery temperature, electric vehicle, lithium-ion batteries, equivalent circuit modeling.

*Corresponding author
Email address: tedjani.mesbahi@insa-strasbourg.fr (Tedjani Mesbahi)

1. Introduction

The energy challenge is one of the main locks to the development of efficient, less polluting and economically viable means of transport with rational use of the world's natural resources. In this context, car manufacturers are undergoing unprecedented technological change [1, 2]. In the transport field, the voices of progress are linked, among other things, to the hybridization and electrification of vehicles. In both configurations, the effective operation of the systems is mainly linked to the availability of the on-board electrical energy and therefore of the battery [1, 3]. The energy storage systems used in the latest generation of hybrid electric vehicles and pure electric vehicles are mainly based on Lithium-ion technology [4, 5]. These batteries have many advantages over old technology of batteries such as high performance and energy density, compact physical measurements, high efficiency in charge and discharge rate, as well as long lifetime, which make them a promising battery for electric vehicle applications. Nevertheless, these characteristics are limited to a range of standard temperature, corresponding air humidity and pressure values [6, 7]. Above these limits, The battery lifetime can be reduced by physical and chemical aging processes that occur inside the cell and are influenced by both the operating strategy and the surrounding conditions (e.g. temperature). In this context, the chemical reactions significantly increase with temperature and with a very high value can cause a phenomena so-called auto-discharge which can lead to a completely loss of capacity. Under low temperatures such as -10 °C the energy performance of the battery drops considerably [8, 9]. It has been reported in the literature that the parameters which determine the capacity and the resistance of the battery depend on temperature and other factors, like state of charge (SOC), current level, and aging. For that, lithium-ion batteries performances highly depend on temperature in electric vehicle application [10, 11, 12]. In this regards, particularly for car manufacturers, electro-thermal modeling accurately batteries is strategic for a better battery packs sizing, a cooling systems design and also for embedded Battery Management Systems (BMS) to ensure an optimal driving

range [10, 13]. In recent years, several battery models are being introduced and studied. They can be classified as electrochemical, mathematical, electrical, and semi-empirical. All these models have the ability to predict the performance of the battery, but with different levels of accuracy [14, 15]. In some instances, the models are usually computationally complex and time consuming, as well as, a large number of parameters and experimental tests are needed for identification, and some of the parameters are extremely hard to obtain [16, 17]. The aim of this paper is to build an electro-thermal model which allows calculating the temperature distribution across the battery cell. The proposed model integrates the electrical and thermal aspects of one battery cell into the same algorithm. This solution helps to analyze heat generation and temperature distribution in the lithium-ion battery for electric vehicle applications. Three thermocouples sensors embedded inside the battery were used to measure the cell-level temperature on the surface arising from current evolution. This paper has been organized as follows. Section II details the design of experiment. Section III presents the equivalent circuit model of lithium-ion battery. The thermal model of battery has been discussed in Section IV. Section V presents the obtained results for three different configurations. Section VI offers conclusions and a description of future work.

2. Design of experiment

The battery studied in this paper is a 40 Ah graphite/nickel-manganese-cobalt-oxide (NMC) pouch cell. The latter is commercialized by $KOKAM$ manufacture under the references $SLPB - 100216216H$. The nominal, maximum, and cutoff voltages of the battery under study are 3.7, 4.2, and 2.7 V, respectively. The maximum continuous charge current is 120 A (3C) while the maximum continuous discharge current is 320 A (8C) . It can support a peak discharge of 480 A (12C) during less than 10 seconds. The operation temperature range for charge is comprised between [0-45] °C and for discharge [-20 -60] °C [18, 19]. The top view from cell thick direction and the cell dimensions are

shown in Fig. 1. The length and width of the main body are 212 mm and 222 mm, respectively. Positive and negative tabs locate at the same front side of the cell [18, 19]. The figure on the left is a picture of the real battery with three sensors. This is noted since the coming results are shown for the equivalent node to the position of each sensor. Sensor (a) will be represented by 'foil right top', sensor (b) 'foil center' and sensor (c) 'foil left bottom'.

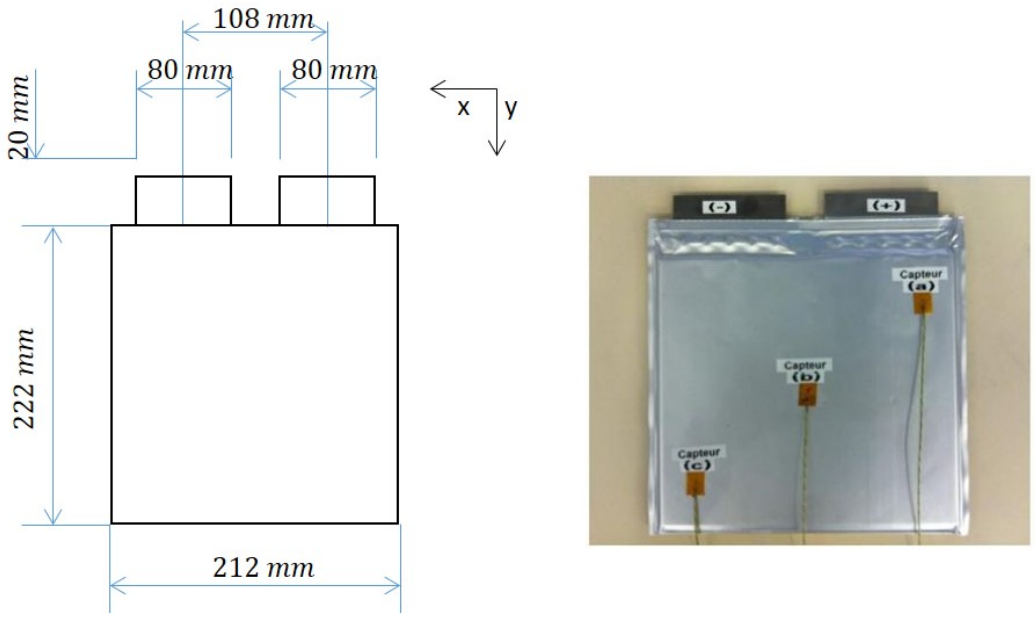

Figure 1: Layout of the laboratory battery on the right and position of the sensors on the left.

An urban electric vehicle ($BolloréBluecar$) was selected for this study. The characteristics of this vehicle are described in detail in [1, 7, 19] The model parameters of the lithium-ion battery is established by using experimental data from laboratory tests and a hybrid particle Swarm–Nelder–Mead optimization algorithm [1, 7]. The laboratory test bench is shown in Fig. 2, the bench includes two main components: a climatic chamber and charge/discharge power system. The power that can be delivered by this bench in continuous operation is 10kW, by using a programmable power supply. The latter is connected to a reversible four-leg power converter (60V/ 600A). The $FPGA$ compact $RIONICRIO -$

9012/9014 real-time control system with *labview* software is used for setting up the test procedure and for data acquisition. Battery cells are placed in climatic chamber in order perform the test at controlled temperature conditions. These units can change the temperature from 0 to 100 °C and are able to change the temperatures at a rate of 3 0.02°C.

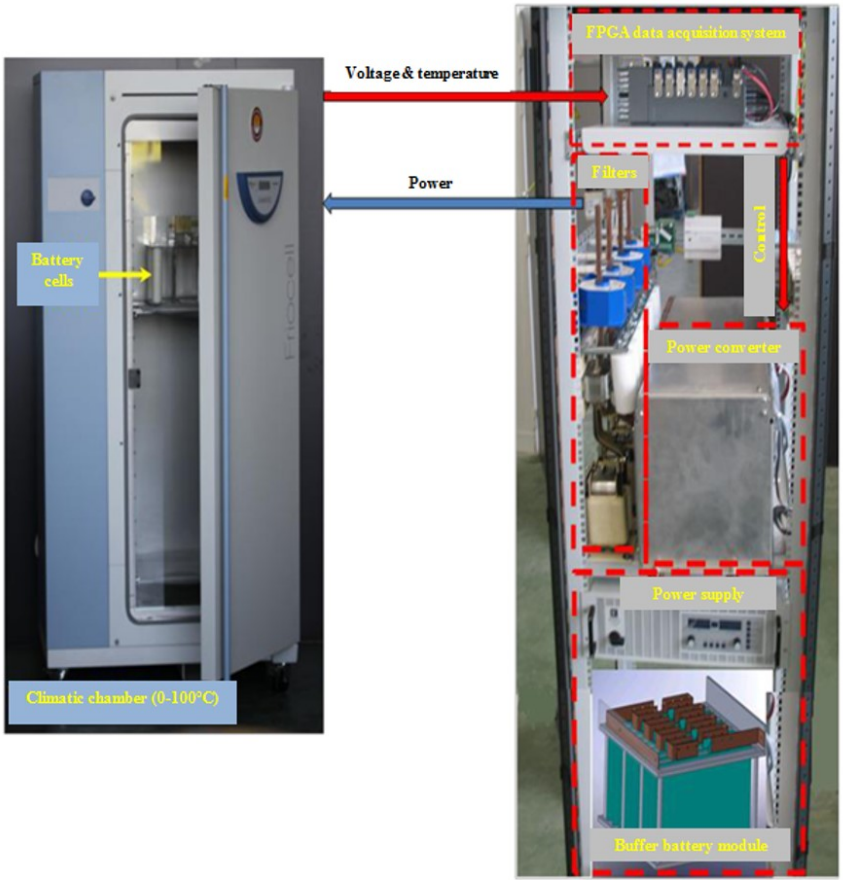

Figure 2: Laboratory test bench.

In order to obtain the model parameters of the lithium-ion battery and verify the accuracy of the model, the common $ARTEMIS$ driving cycle is chosen for testing the urban electric vehicle powered by a lithium-ion battery energy storage system based on KOKAM NMC pouch cell ($SLPB - 100216216H$). This cycle consists of both urban and road driving parts with an average speed

of about 7.5 and 110.7 km/h, respectively. The combination of urban and road cycles can simulate a rolling distance of 22 km over a period of about 34 min. To achieve a total driving range close to 154 km, the ARTEMIS driving cycle has been repeated seven times with an average roadway slope of 2.5% [7, 19]. Based on the constraints ensured by the battery pack,the sizing algorithm has been developed, which is described in detail in [7, 19]. The inputs parameters of this algorithm are the characteristics of the battery cells and electric vehicle mission defined by the speed profile and the slope of the roadway. As a result thereof, the sizing algorithm can defined the number of cells that gives the characteristic of the battery pack (power limits in charge and discharge, pack capacity, weight, volume, and cost). To simplify the real current profile requested by the electric vehicle and using it to identify the the model parameters,in our laboratory, a heuristic method based on constraints classification in intensity levels has been developed [1]. It aims to reduce the cycling time while preserving the most important characteristics for test profiles such that the maximum value of the current and the amount of exchange charges [7].

Although in this study only the electric and thermal model are studied, there are three levels of modeling that must be taken into account to simulate the overall behaviours of a lithium-ion battery. Electrical, thermal and aging models can present these levels. Electrical modeling is necessary to present voltage variation, and state of charge (SOC) during battery operation, thermal modeling is required to estimate the evaluation of battery temperature and aging model can predict the impact of operating conditions on the battery lifetime [1, 7]. These three models work in one loop. Initially the battery has an impedance that will change with temperature and aging. The thermal model is coupled to the electrical model since the heat production based on joule losses is calculated by the electrical model. The inputs of the thermal model are this power and the ambient temperature. With the thermal model the internal temperature is calculated and will be as well an input for the electrical model due to the dependence of its parameters on it. The other inputs of the electrical model are the load profile that can be power or current. This model defines the

voltage, the SOC and the current which are the inputs of the aging model along with the temperature [1]. The aging model updates the value of capacity and resistance that will be used for the next step, when the cycle restarts with this new impedance.

3. Equivalent circuit model of lithium-ion battery

Electrical models, accuracy of which lies between electrochemical and mathematical models are electrical equivalent models using a combination of voltage sources, resistors, and capacitors for co-design and co-simulation with other electrical circuits and systems [7, 12, 7, 20].

3.1. Proposed Battery Model

For this study, equivalent circuit based models are chosen to study the electro-thermal behavior of the battery. In this context, to model the electric behaviour of the battery different types of RC equivalent circuits can be used. The most appropriate in this case (NMC pouch cell) is composed of a voltage source which represents the open circuit voltage, a resistor which represents the ohmic resistance in the cell and two parallel branches that models the chemical diffusion in the cell. A schematic of the circuit can be seen in Fig. 3.

Depending on the approach and the precision to achieve, the parameters of the circuit can be function of SOC, temperature etc [7, 20]. These parameters can be estimated with different methods, mainly with experimental tests like electro-chemical impedance spectroscopy (EIS) or with measurements of the current profile and voltage response of the battery, using a method of optimization to identify the electrical parameters. The equivalent circuit used in this paper is an extension to the *Thevenin* classical model which is suitable for electric power applications. It consists in an open-circuit voltage (OCV) associated with a nonlinear complex impedance composed of three elements. V_{ocv} changes according to SOC and the voltage drop across battery internal resistance R_Ω relates to the SOC and the current sign. The voltage across the R_{dll}, C_{dll},

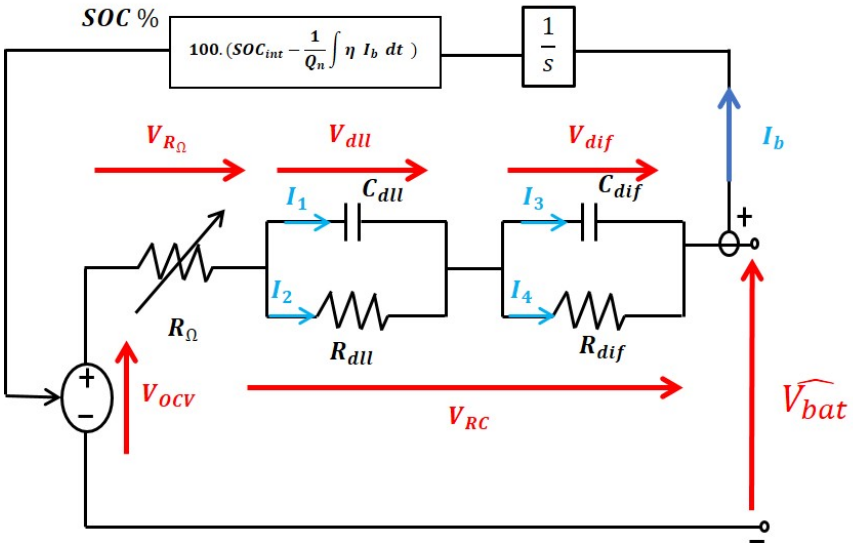

Figure 3: Equivalent circuit model of lithium-ion battery.

R_{dif} and C_{dif} circuits simulate the polarisation process of the battery during charging and discharging caused by charge transfer, diffusion and double- layer capacitance phenomena. For further details about the equivalent circuit based model, readers can be referred to [1, 7].

3.2. Parameters identification experiments

In this paper, the cell was put into an climatic chamber during the test to keep the ambient temperature constant (23 °C), and then, discharge pulses based on *ARTEMIS* simplified laboratory driving cycle were applied to the battery cell by using the laboratory test bench. Previously, the battery has been recharged according to the strategy of constant current and constant voltage (CC-CV) defined by the manufacturer. The temporal identification method based on a hybrid (PSO/NM) optimization algorithm was used to identify the parameters of the lithium-ion battery model . This improved method of the characterization is based on the use of equivalent current profiles applied to the traction battery in real applications [1, 7]. This solution enables us to evaluate

directly the impedance of the battery in real time and at several working points, without performing additional tests. In such case, the optimization searches the best fitting parameters which give the less error between the real measure of the voltage and the simulated voltage by the equivalent circuit, using the hybrid (PSO/NM) optimization algorithm.

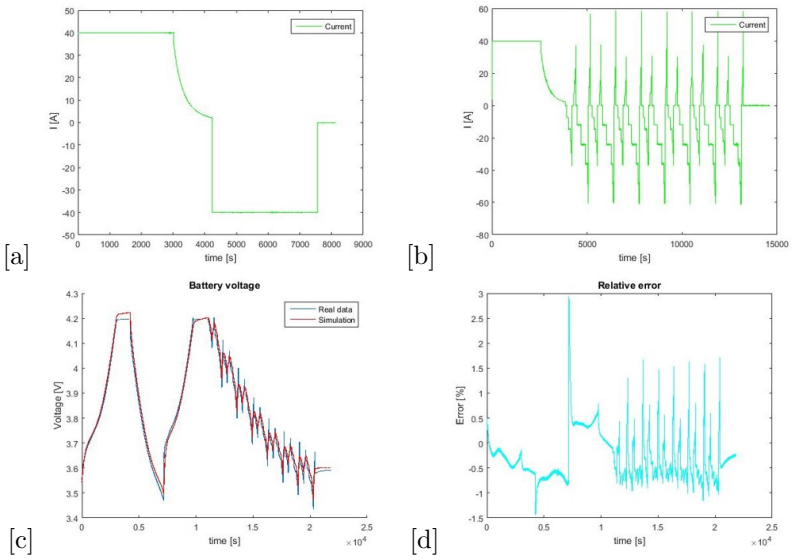

Figure 4: Experimental results: (a) Current profile for test 1C charge discharge; (b) Current profile for 1C charge and cycling of the laboratory battery based on ARTEMIS driving cycle; (c) Simulated and measured voltage for both tests coupled ; (d) relative error .

Fig. 3(a) illustrates the first test that consists of a typical profile of 1C charge and discharge, using in the charge, the protocol of the manufacturer with a period of constant current (CC) and then a constant voltage (CV), when the maximum value of the voltage is reached. The initial SOC is 10 % and it is charged to 100 % to later discharge it up to 10% as well.

Fig. 3(b) shows the current profile presents one mission of 154 km vehicle driving range (80% of depth of discharge (DOD)) followed by a charge phase of constant-current– constant-voltage (CC/CV). Fig. 3(c) illustrates the comparison of the modeling and experimental voltage of the lithium-ion battery cell for a given current profile (two coupled one after another). It can be very

clearly seen that the voltage behavior of the lithium-ion battery can be simulated thanks to the proposed model. The comparison shows that there is no global divergence between both responses and the total error band is <3%, as shown in Fig. 3(c) comparison between the voltage responses of real battery cell and model one. This comparison shows that there is no global divergence and no great mismatch between measured and simulated points.

3.3. Distributed RC equivalent electric model

The model is made for a pouch (NMC) lithium-ion battery in electric vehicle applications. This is quite important, since the model takes into account the geometry of the battery. Pouch batteries consist of two tabs and the foil. The positive tab is a plate usually made of aluminium whereas the negative tab is made of copper. The foil is a more complexed element. It contains several layers of five components: the positive and negative plates of the foil, the positive and negative material and the separator. Consequently the current in the foil flows from one plate to another through the internal layered structure (axe Z) and within the plate (axes X and Y). However in the tabs the current just flows in each horizontal plate (axes X and Y). Therefore the modeling of the tabs and the foil is a bit different. To calculate the parameters in different points of the battery, each part (positive tab, negative tab and foil) is divided into a number of rows (n) and a number of columns (m) which gives the number of nodes in the mesh of the battery. As mentioned above the foil is composed of a layered structure, therefore, the modeling is divided in two parts. On one hand, the positive and negative plates of the foil are modelled with electric resistances in series. On the other hand, the positive and negative material and the separator is represented by a first order RC equivalent circuit model. As there are $n \times m$ nodes, this part is divided into $n \times m$ parallel branches of this model connected to the nodes, finally having $n \times m$ sub-models. The tabs are modelled with electrical resistances in series. The current flowing from the negative plate to the positive plate of the foil is obtained solving the electric circuit of each sub-model:

$$i_{i,j} = \frac{u_{ocv(i,j)} - (\varphi^{+}_{(i,j)} - \varphi^{-}_{(i,j)}) - u_{p(i,j)}}{r_{\Omega(i,j)}} \tag{1}$$

$$C_{p(i,j)} = \frac{du_{p(i,j)}}{dt} = i_{(i,j)} - \frac{u_{p(i,j)}}{r_{p(i,j)}} \tag{2}$$

where the sub-index i and j represent the position of each sub-model in the i_{th} row and j_{th} column. u_{ocv} is the equilibrium potential of the sub-model, φ^{-} is the node potential of the negative foil, φ^{+} is the node potential of the positive foil, r_{Ω} is the ohmic resistance of the sub-model, u_p the the voltage across the parallel branch inside the sub-model and c_p and r_p the capacitance and resistance in this parallel branch which represent the chemical diffusion in the cell.

$Kirchhoff's$ first current law can be applied now in the nodes of the plates, where the sum of currents flowing into one node is equal to the sum of currents flowing out of that node.

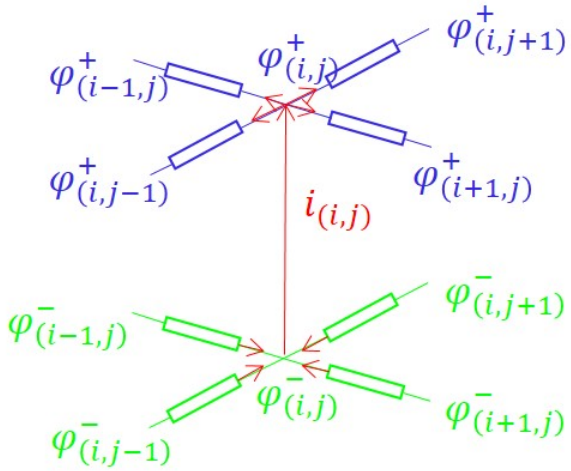

Figure 5: Current through the plates.

Consequently in the positive / negative plate the equation reads:

$$\begin{cases} r_{+i(i,j)} = 4\varphi^{+}_{(i,j)} - \varphi^{+}_{(i-1,j)} - \varphi^{+}_{(i+1,j)} - \varphi^{+}_{(i,j-1)} - \varphi^{+}_{(i,j+1)} \\ r_{-i(i,j)} = 4\varphi^{-}_{(i,j)} - \varphi^{-}_{(i-1,j)} - \varphi^{-}_{(i+1,j)} - \varphi^{-}_{(i,j-1)} - \varphi^{-}_{(i,j+1)} \end{cases} \tag{3}$$

where r_+ and r_- are the electrical resistances in the positive and negative plate between the adjacent nodes. The values of the resistances within each plate are considered to be the same since the length of each element in axes X and Y will be calculated to be equal and the material is homogeneous along it. To solve this problem, the equations of the current are coupled and a matrix system is built. Firstly, the connection between the nodes is defined with a function which generates the matrix A^+ for the connections within the positive foil and positive tab and A^- with the connections between the negative foil and negative tab. The methodology to build this matrix is explained below. The vectors ϕ^+, ϕ^-, I, E and V_p are defined and contain the values of φ^+, φ^-, i, u_{OCV} and u_p for all the nodes. The equations in the matrix form are written as:

- *Current in the positive and negative plates* :

$$\begin{cases} r_{+I} = A^{+}\phi^{+} \\ r_{-I} = A^{-}\phi^{-} \end{cases} \tag{4}$$

- *Current in the sub-models*

$$R_\Omega I = E - (\phi^{+} - \phi^{-}) - V_p \tag{5}$$

where R_Ω is a diagonal matrix whose diagonal contains the values of r_Ω for all the nodes. The system is solved as if the tabs have also sub-models, therefore the values of r_Ω corresponding to the tabs are set to infinity. To accelerate the numerical computation the vector G_Ω is introduced, where the *ohmic* admittance of the tabs are set to zero.

$$G_\Omega = R_\Omega^{-1} \tag{6}$$

The equations are coupled in order to solve the node potentials $\phi^+$and ϕ^-

$$\begin{cases} \frac{A^+\phi^+}{r_+} = G_\Omega(E - \phi^+ + \phi^- - V_p) \\ \frac{A^-\phi^-}{r_-} = G_\Omega(E - \phi^+ + \phi^- - V_p) \end{cases} \tag{7}$$

Gathering the terms in matrix form, the expression obtained is:

$$\frac{A^+}{r_+} + G_\Omega - G_\Omega - G_\Omega\frac{A^-}{r_-} + G_\Omega\phi^+\phi^- G_\Omega(E - V_p) - G_\Omega(E - V_p) \tag{8}$$

To resolve this system, boundary and initial conditions must be defined. There are two boundary conditions: the current is imposed at the edge of the positive tab where all the nodes share the external current evenly and the node potentials at the edge of the negative tab are set to zero. As the values of E, V_p and R_ω depend on the state of charge (SOC), the initial value of E is equal to the open circuit voltage for $100\%SOC$, the values of R_Ω are calculated using the lumped value of the first order RC equivalent electric circuit multiplied by the number of nodes in the foil and for the first iteration the values are the corresponding to $SOC = 100\%$. V_p is set to zero for the first iteration, and then is updated at each iteration according to equation eq:3. Therefore this equation is discretised using the Euler method, which could be defined as:

$$u_{p,t+\Delta t} = u_{p,t} + \frac{i_t r_{p,t} - u_{p,t}}{r_{p,t}c_{p,t}}\Delta t \tag{9}$$

where Δt is the step time. Rewriting it in the matrix form:

$$V_p^{t+1} = V_p^t + \Delta t[C_p^t]^{-1}I - V_p^t\Delta t[C_p^t]^{-1}[R_p^t]^{-1} \tag{10}$$

where $[C_p]$ is a diagonal matrix whose diagonal contains the capacitance values, C_p, of the sub-models in the foil. The C_p values are calculated using the lumped value of the first order RC equivalent electric circuit divided by the number of sub-models. $[R_p]$ is another diagonal matrix whose diagonal contains the resistance values, R_p, of the sub-models. Similarly, the C_p values are calculated using the lumped value of the first order RCequivalent electric circuit multiplied by the number of sub-models. The initial values of the matrix are

set for100%SOC. After obtaining the node potentials, the power losses in the plates can be calculated according to the next expressions: Heat generation rate of the k_{th} node in the positive foil and tab:

$$\dot{q}_k^+ = \sum_{i=1}^{N} = \frac{A^+(k,i)(\varphi_k - \varphi_i)^2}{2r_+} \tag{11}$$

where N is the number of nodes in the positive plate.

Heat generation rate of the k_{th} node in the negative foil and tab:

$$\dot{q}_k^+ = \sum_{i=1}^{N} = \frac{A^-(k,i)(\varphi_k - \varphi_i)^2}{2r_-} \tag{12}$$

where N is the same number of nodes in the negative plate.

3.4. Mathematical resolution

The most important part is to create the function connection which gives the node connections in matrix form. The easiest way is to develop a function which gives the connectivity between an individual plate for a given number of rows and columns and then couple the different plates (tabs and foil). The matrix will have a dimension of n-rows times m-columns. The next figure represents a general case, which is used as an example of how the function works.

The blue circles represent the number of nodes that a plate will have. Depending on the position of the node the connections are different. From the figure it can be seen that there are nine possible cases where the node can be placed.

The matrix (A) is organized as follows: each row represents one node and the columns of each row the nodes at which the current node can be connected to. The function gives a value of one if the nodes are connected and a zero if they are not. The function has two loops whose indexes are $i = 1 : n$ for the rows and $j = 1 : m$ for the columns. The current node is defined by its position in the plate:

$$k = (i-1) \times m + j \tag{13}$$

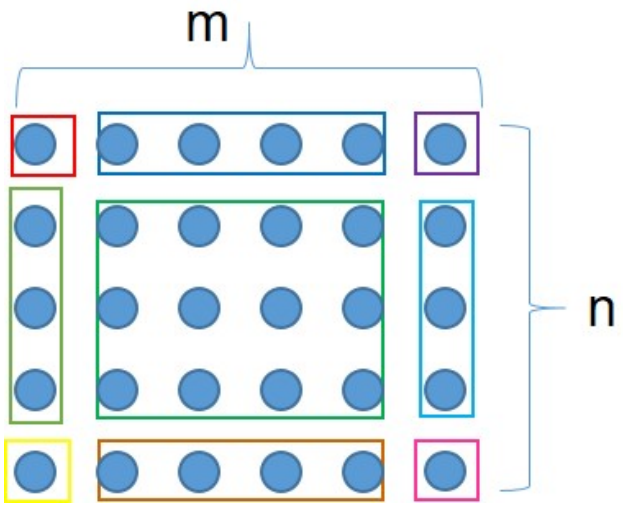

Figure 6: Connectivity of the nodes.

The current node can be connected to a maximum of four nodes, therefore there are four statements and depending on the case one are used or another. If the node is connected to another on its left, the if case includes this statement:

$$A((i-1)\times m+j,(i-1)\times m+j-1)=1 \tag{14}$$

If the current node is connected to another on its right, the if case includes the statement:

$$A((i-1)\times m+j,(i-1)\times m+j+1)=1 \tag{15}$$

If the current node is connected to the node above it, the if case includes the statement:

$$A((i-1)\times m+j,(i-2)\times m+j+1)=1 \tag{16}$$

And finally, if the current node is connected to the node below it, the if case includes the statement:

$$A((i-1)\times m+j,i\times m+j)=1 \tag{17}$$

Introducing in the function the number of rows and columns, the connective matrix is automatically built. For the battery, it will generate two matrices: one

for the foil, of dimensions $n_f \times m_f$, and another one for the tab, of dimensions $n_t \times m_t$. Now the matrices A^+ and A^- can be obtained coupling the generated matrices for each plate (foil and tab). As the matrices A^+ and A^- are used to write the equations eq:3 and eq:4, in matrix form equations eq:5 and eq:6, it is necessary to add a diagonal (at the moment zero) to each generated matrix. The values of the diagonal are the sum of each row with the contrary sign. To adapt the matrix to the sign convention adopted in equations eq:3 and eq:4 the matrix is multiplied by -1. As regards matrix A^+,it is going to to contain the connections of the nodes in the positive foil and positive tab. As the positive foil and positive tab share several nodes, the generated matrix cannot be coupled directly. The number of nodes and the dimension is N which is equal to $n_f \times m_f + (n_t\text{-}1) \times m_t$. A new parameter, j_{s1}, is added to place the tab. Fig 7 shows how the nodes are organized in the positive foil and tab.

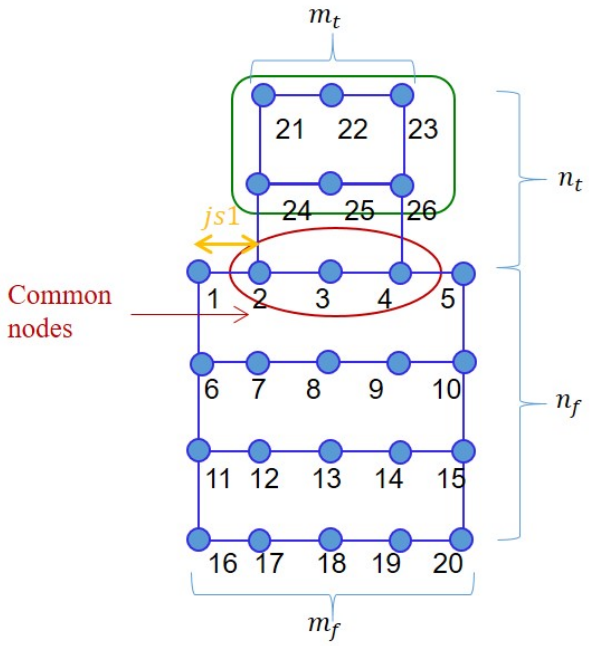

Figure 7: Discretization of the positive plate.

The new matrix is organized as follows; the connective matrix of the foil

is copied directly on the top far left. On the bottom far right, the connective matrix of the tab is partially added $(1 : (n_t - 1) \times \mathrm{m}_t, 1 : (n_t - 1) \times \mathrm{m}_t)$ positions. The left columns and rows of the connective matrix of the tab are added in the new matrix to define the connections of the positive foil and the positive tab. The rows $((n_t - 1) \times \mathrm{m}_t : n_t \times \mathrm{m}_t, 1 : (n_t - 1) \times \mathrm{m}_t)$ are placed on the right of the connective matrix of the foil and represent the connections between the common nodes (defined in the foil) with the nodes of the tab. The columns $(1 : (n_t - 1) \times \mathrm{m}_t, (n_t - 1) \times \mathrm{m}_t : n_t \times \mathrm{m}_t)$

are placed under the connective matrix of the foil and represent the connections of the tab with the common nodes (defined in the foil). Fig 8 displays clearly how the matrices are coupled. The matrix A^- is built similarly with the

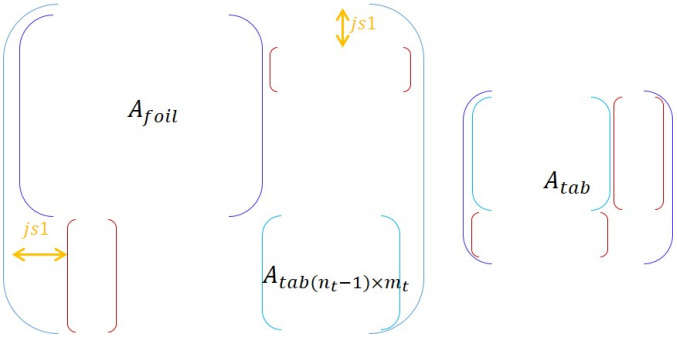

Figure 8: Disposition of the matrix A^+(positive plate).

same methodology but taking into account that the negative tab is placed in the other side.

The boundary condition of the current is simply imposed introducing the value of the current divided by the nodes in the positive edge of the tab in the independent vector of the equation eq:8. To impose the node potential equal to zero in the edge of the negative tab, the matrix A^- is modified. The values of the rows that correspond to the nodes at the edge of the negative tab are set to zero except for the connection with its own which is set to 1. Then in the independent vector of the equation system, the corresponding values to the edge of the negative tab are set to zero. The number of nodes should not be

chosen arbitrarily but taking into account the geometry of the battery. Either the number of nodes in the foil determines the number of the nodes in the tab or vice versa. This is done to maintain the geometrical proportions between the foil and the tab. In the same way, either the number of rows determines the number of columns or vice versa. This is done to have elements with the same length and width which allows having the same value of the electrical resistances in the axe X and axe Y. In the following figure the layout of the standard NMC battery is displayed. For further details about how to proceed with the definition of the proportional rapport between the width of the foil and the tab, readers can be referred to [9]

4. Thermal model of lithium-ion battery

The aim of the study is to calculate the temperature distribution of the battery, therefore this part is explained in detail. *As* it was said before the electrical model and the thermal model are coupled directly to introduce straightly the outputs of the electrical model into the thermal model. The energy balance in the battery is governed by the general heat equation.

$$\rho c V \frac{dT}{dt} = \dot{Q}_{gen} + \dot{Q}_{in} - \dot{Q}_{out} \tag{18}$$

where ρ is the density of the battery, c the specific heat capacity, V the volume of the battery and T the temperature of the battery. ($\dot{Q}_{gen}$) represents the generated heat and ($\dot{Q}_{in}$-$\dot{Q}_{out}$) the transferred heat by conduction and convection. The generated heat is produced from two sources: chemical reactions and conduction of electrical charges. The first one is a reversible thermodynamic effect caused by the entropy changes of the cell reaction and the second one is an irreversible effect due to *Joule* heating losses. This is written by:

$$\frac{\dot{Q}_{gen}}{dt} = i(t)[T\frac{dQ_{ocv}}{dt} + u - u_{ocv}] \tag{19}$$

4.1. RC equivalent thermal model

To calculate the temperature, the equivalent thermal model consists of implementing the thermal circuit as if it was an electric circuit. The analogy is as follows: the thermal resistance has the same behavior than an electrical resistance; the temperatures are modeled as if they were voltages and the heat is represented as a current. Therefore the general equations of an electric circuit are used:

- *Current across a capacitor:*

$$i_c = \frac{dv}{dt} \iff q_c = \frac{dT}{dt} \tag{20}$$

- *Current across a resistor:*

$$i_r = \frac{du}{R} \iff q_r = \frac{T}{R} \tag{21}$$

According to this analogy, heat capacities are used to model the ability to hold thermal energy whereas thermal resistances model the heat flow within the cell and to the ambient. The losses are modelled by a current source, where the three components of the equation eq:16 are identified: the generated heat with a current source, the stored heat with a capacitor and the transferred heat with a resistance. The ambient temperature is represented with a voltage source. Based on the distributed RC equivalent circuit, the distributed equivalent circuit is built, where the generated heat (losses) and the temperature are calculated in each node. Now the equations must be written for each node followed by the matrix form. It has to be noted that in the tabs there are not sub-models, therefore there are not generated heat. Nevertheless, the transferred heat by convection will be taken into account in the tabs. In the foil the generated heat is calculated with the the equation eq:17 applied to each node:

$$q_{g,k} = i_k \times (u_{ocv\,k} - (\phi_k^+ - \phi_{(k)}^-)) + i_k T_k \times \frac{\partial u_{ocv}}{\partial T} \tag{22}$$

where the first term represents the irreversible heat and the second term the reversible heat as it is just been stated. To calculate the entropy change the

method proposed by [12, 13] is chosen. In matrix form the generated heat is written as:

$$\dot{Q}_{gfoil=[I_{foil}]\times(U_{ocv}foil}-(\phi^{+}_{foil}-\phi^{-}_{(foil)}))+[I_{foil}]\times T_{foil}\times\frac{\partial u_{ocv}}{\partial T} \tag{23}$$

where $[I_{foil}]$ is the diagonal matrix of the foil part of the current vector calculated with equation eq:4. To this generated heat, the power losses $(\dot{Q}^{+})and(\dot{Q}^{-})$, equations eq:11 and eq:12 must be added in the general equation eq:17. To calculate the transferred heat, $(\dot{Q}^{in})-(\dot{Q}^{out})$) part, equation eq:19 has to be reminded. The analogy current-heat and temperature-voltage implies that the same method to calculate the current is used to calculate the transferred heat . A matrix of connections (A_{th}) within the nodes and the ambient is built where the thermal resistances are considered. The construction of this matrix is explained below. The equation in matrix form reads:

$$\dot{Q}_{in}-\dot{Q}_{out}=[A_{th}]\times T \tag{24}$$

Finally the heat equation to solve reads:

$$[A_{th}]-\dot{Q}_{total}=[mc]\frac{dT}{dt} \tag{25}$$

where $[mc]$ is the diagonal matrix which contains the equivalent mass and heat capacity of the tabs and foil and $(\dot{Q}_{total})$ the vector that contains all the losses. Applying the *Euler* method to solve the differential equation:

$$A_{th}\times T^{k-1}-\dot{Q}_{total}=-[mc]\times\frac{T^{k+1}-T^{k}}{\Delta t} \tag{26}$$

which leads to the equation

$$T^{k-1}=(A_{th}+\frac{[mc]}{\Delta t})^{-1}\times(\dot{Q}_{total}+\frac{[mc]}{\Delta t}\times T^{k}) \tag{27}$$

4.2. Mathematical resolution

As the dimension of the vectors is not the same, a new mesh for the thermal model is set. In the electrical model, the mesh was done for two plates, the positive (positive tab and foil) and the negative (negative foil and tab). As in

the thermal part there is not a positive and a negative part, the mesh is done for the three elements together (positive tab, foil and negative tab). The number of nodes in each element is the same than in the electric model ($n_t \times m_t$ and $n_f \times m_f$), the only difference is the global number of nodes $M : 2(n_t - 1) \times m_t + n_f \times m_f$. Therefore all the vectors must have this dimension. The arrangement of the vectors is also changed, placing firstly the values of the positive tab, followed by the foil and in last position the negative tab. This implies that the vectors used in the thermal part will be adjusted adding zeros in the respective positions where they have not value. The vector (Q_g) has $(n_{t-1}) \times m_t$ zeros, followed by the vector $(\dot{Q}_{(g_{foil})})$ followed by $(n_t - 1) \times m_t$ zeros. For $((\dot{Q}^+)$) and $(\dot{Q}^-)$ the $(n_t - 1) \times m_t$ zeros are added at the end and at the beginning of each vector respectively.

To calculate the transferred heat,$\dot{Q}_{in} - \dot{Q}_{out}$ part (equation eq:22), the matrix of connections, A_{th}, is created with the previous instructions. In this case the matrix has a dimension of $(M + 1 \times M + 1)$. Therefore, the M first rows and M first columns represent again the connections between the adjacent nodes, and each value $(1 or 0)$ is divided by the thermal equivalent resistance of the tab or the foil depending on the node position. The last column added represents the connection of each node to the ambient, hence, all the values of the column will be 1 (because all nodes are connected) divided by the equivalent resistance in the axe Z (containing the conduction and the convection). The diagonal of the matrix is the sum of each row as before. To maintain the sign criterion adopted before, the final matrix is multiplied by -1. The only thing remaining to determine is the last row added to impose the ambient condition. All its values are zero except for the last position which is set to 1. In the next figure it can be seen the organization of the matrix A_{th}.

4.3. Disposition of the matrix A_{th}

To consider the new dimension $(M + 1)$ after adding the ambient condition a new vector of losses is created $\dot{Q}_{total}$ with the dimension M+1. The first M elements correspond to the sum of the vectors $\dot{Q}_g$, $\dot{Q}^+$ and $\dot{Q}^-$ and in the last

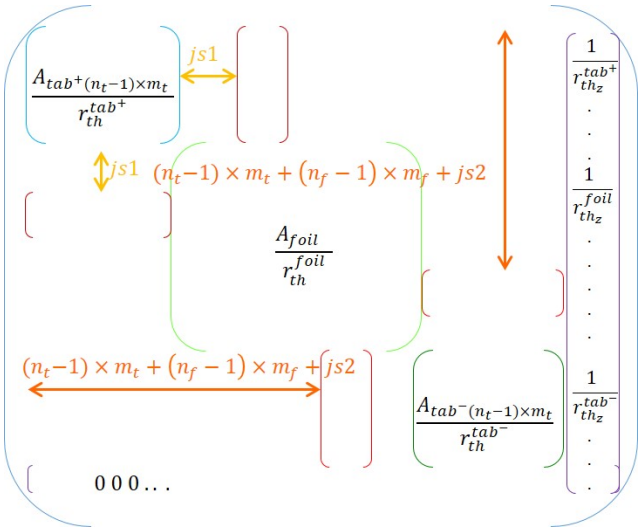

Figure 9: Disposition of the matrix A_{th} .

position the ambient temperature is set. Consequently when equation eq:25 is solved, the vector T will have also a dimension of $M+1$, being the last value the ambient temperature.

5. Results and discussion

As it was explained in the beginning, the electrical and thermal model work in a loop where the outputs of the electrical model enter in the thermal model and then the output of the last one, the temperature, allows updating some electrical values, since the electrical performance differs depending on the temperature.

Fig. 10(a) represents the voltage of the battery in function of the capability for different temperatures. On one hand, the capability expresses the percentage of the nominal capacity that can be used for each temperature. In other words, if the temperature is lower than the normal condition (25 °C and 100 % capability) the real capacity of the battery is lower than the nominal capacity, and this implies that for a given profile of the current the state of charge reaches 0 before, consequently, the duration of the battery is reduced because

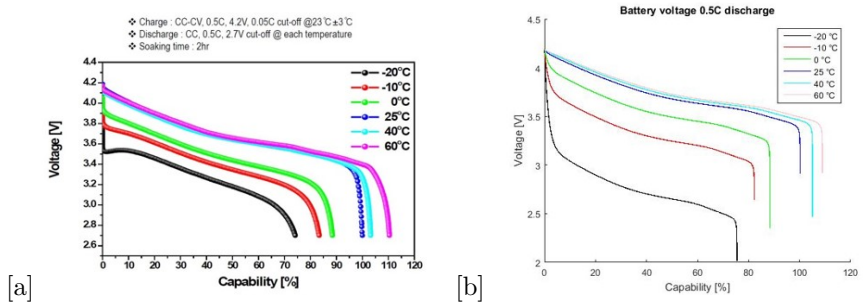

Figure 10: Voltage of the battery in function of the capability for different temperatures: (a) Experimental results of KOKAM-manufacturer (data sheet): Voltage curves for 0.5C discharge at different temperatures ; (b) Simulated voltage curves for those temperatures .

the energetic capacity is lower. In contrast to, if the temperature is above the standard condition the nominal capacity increases and therefore the state of charge reaches zero later, the opposite occurs, the duration of the battery is increased.

As it can be seen from the Fig. 10(b), the performance for the temperatures from -10 °C to 60 °C is quite accurate. However the behaviour for a temperature of -20 °C distances from the real results given in the data sheet. Therefore, for this last condition the model probably will not behave properly. To analyze heat generation and temperature distribution in the lithium-ion battery, the number of nodes is chosen taking into account the dimensions of the battery to maintain the rapport between the width and length of each element in the foil and the tab as it was detailed before. The program developed in MATLAB is executed with the current of the first test with and calculates the SOC at each iteration after updating the value of the energetic capacity and consequently the parameters of the equivalent electric circuit. To verify that the model works over the time, the terminal voltage is measured in different nodes between the positive and negative tab and across the positive and negative foil, although experimentally this cannot be measured.

Fig. 11(a) displays the simulated voltage compared to the experimental data. Coherently all the curves of the model are practically the same.From Fig. 11(b),

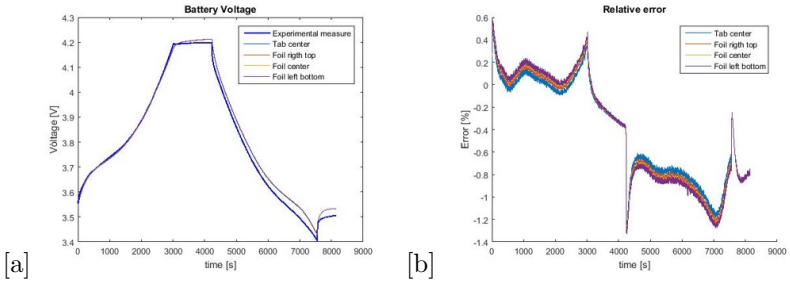

[a] [b]

Figure 11: Experimental and Simulation results: (a) Battery voltage in different nodes ; (b) Relative error .

the relative error between the different nodes and the real measure is shown whose maximum value is 1.4 %. From Fig. 12, it can be seen that the differences

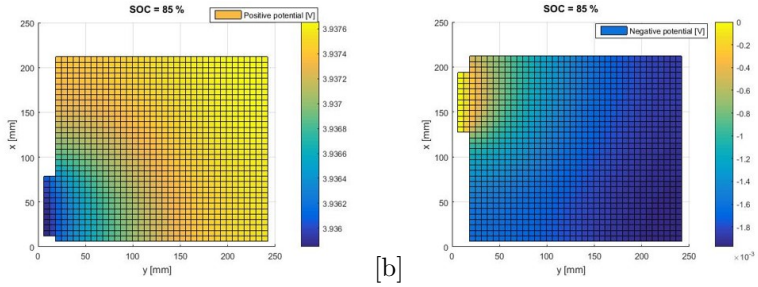

[a] [b]

Figure 12: Simulation results at t=4842 seconds: (a) Positive potential distribution ; (b) Negative potential distribution .

are indeed insignificant, as it was expected after seeing the curves of the voltage in different nodes. In fact the potential should be the same in all points. In Fig. 13 the current density is displayed. The later is calculated dividing the current of each node by the surface of the element. It can be appreciated that the higher absolute values of the current correspond to the lowest of the potential. However, the difference is also minor. The dissipated losses in each plate have a small value (10^{-4}) compared to the generated losses (10^{-3}); hence the latest is the essential part which contributes to the evolution of the temperature.

From Fig. 14, it can be seen that the curve goes down when the current decrease until zero. The small depths in the charge and discharge phases corre-

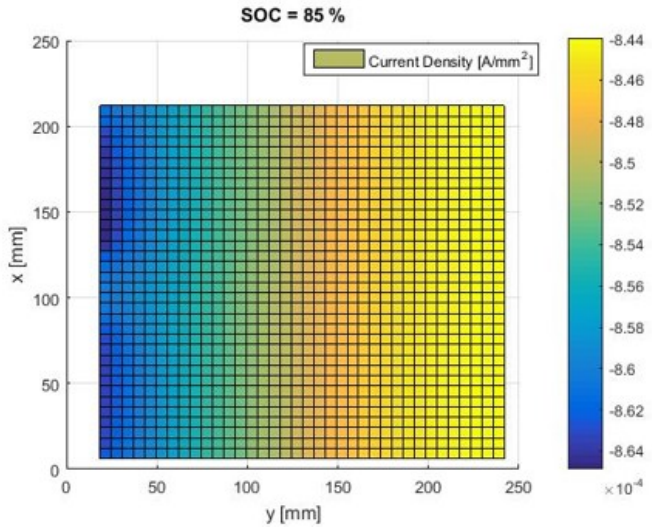

Figure 13: Current density distribution at t=4842 seconds.

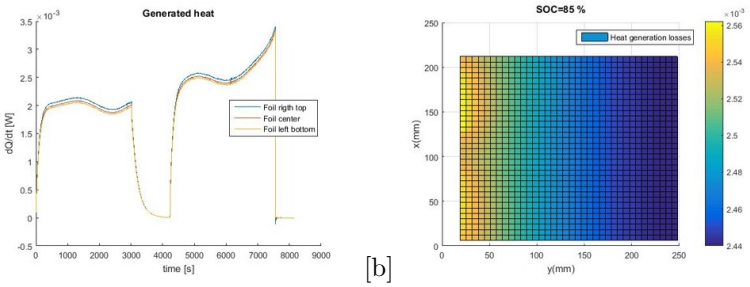

[a] [b]

Figure 14: Simulation results at t=4842 seconds: (a) Generated heat evolution; (b) Generated heat distribution .

spond to the change of entropy of the reactions in the cell (the reversible heat). The distribution of the generated heat is in accordance with the current density distribution with higher values near the tabs. The distribution is maintained along the time as it can be seen from the curves where the highest generation is for the nodes in the right top of the foil and the lowest in the left bottom part of the foil. Nevertheless it can be noted that the differences are not very pronounced.

As it is appreciated from Fig. 15, the temperature is quite homogeneous

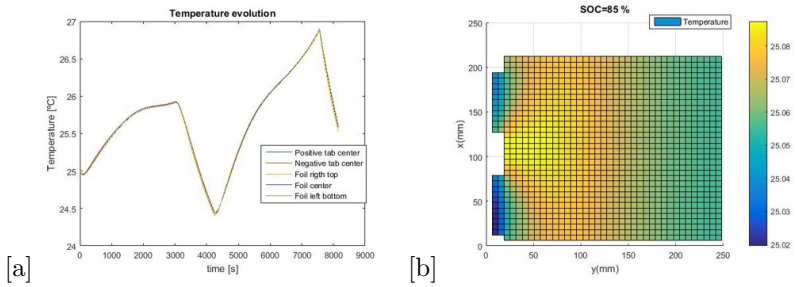

Figure 15: Simulation results at t=4842 seconds: (a) Temperature evolution ; (b) Temperature distribution .

across the battery with a negligible difference of less than 0.1 °C. The simulated values are compared to the measured ones in Fig. 16.

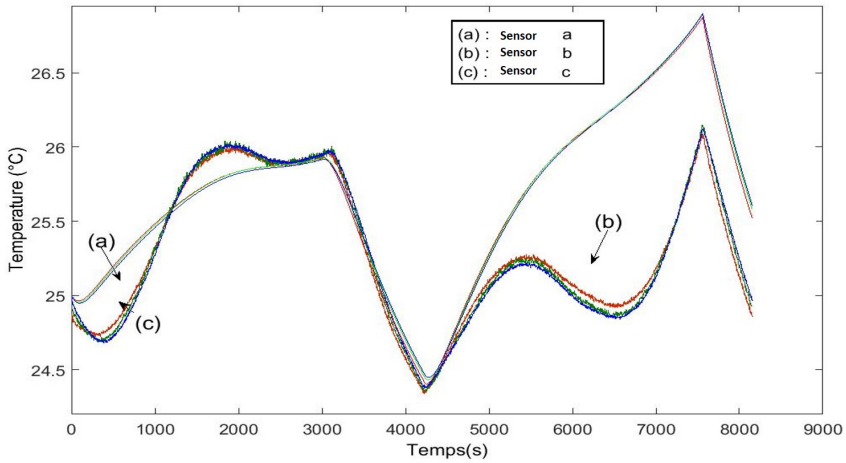

Figure 16: Comparison of the temperature of the three sensors with the simulated .

Red lines corresponds to the sensor a, green lines to the sensor b and blue lines to the sensor c (see Fig. 1). From Fig. 16) it can be seen that even the simulated temperature and the experimental do not match accurately, the tendency is obtained, and the maximum difference is 1.35 °C. Besides, enlarging the image it can be appreciated that the three lines representing the three nodes are in the same order than the real measure of the sensors. In the beginning there is a drop in the curve because the initial temperature in the climatic chamber

is 23 °C and in the battery is 25 °C. The model shows a little drop but does not fall so deeply. This must be due to the refrigeration in the climatic chamber where there are fans. In the model the heat transfer parameter considered is for natural convection, therefore this exchange of heat due to the cooling is out of the modeling. In the phase of recharging the experimental data changes the scope and goes a bit down and then goes up again. This effect is due to the entropy changes and Fig. 15 shows that the model takes this into account. However, it seems that the depth in the curve of the generated heat must be higher so that the temperature would behave as the real measure. The issue that the values of the entropy change are not for exactly this battery might cause this error. The discharge phase is where the biggest difference is found. It can be seen too in the generated heat that the entropy changes are important in the interval where the temperature decreases. However, it seems that any other phenomena might cause this drop like the fact that not all the losses have been considered in the simulation and that the electric model is not completely accurate.

6. Conclusion

In this paper, an electro-thermal model for a 40Ah NMC pouch battery cell is proposed.The model is composed of distributed equivalent electric circuits and distributed equivalent thermal circuits which allow calculating the distribution of different parameters, like the potential,current density and temperature.Furthermore, the model includes the feedback of the mean temperature, in the electric model, to recalculate the electric parameters which are function of it. The model is validated for -10 to 60 °C by comparing the simulated temperature with the real results given in the data sheet of KOKAM-manufacturer. In addition, the performance of this model is investigated under a constant current discharge profile with 1C and CC/CV charge protocol.The relative error of simulated temperature compared to measured results at three test points in the pouch battery cell is less than 1.35 °C, indicating that the model can be

applied to predict the internal characteristics at different current solicitation. For future work, the battery electro-thermal model can be expanded to obtain a temperature distribution within the pack over a wider range of temperatures for electric vehicle applications.For that,new experimental tests must be carried out to validate the model for new conditions. Apart from different measures of the temperature in different points with sensors, it would be interesting to obtain real infrared images to validate also the temperature distributions.

Acknowledgment

The authors would like to express their appreciation to Dr, Nassim Rizoug, S2ET-ESTACA-Laval, France for providing technical assistance and battery experimental tests.

References

[1] T. Mesbahi, N. Rizoug, P. Bartholomeus, R. Sadoun, F. Khenfri, P. Le Moigne, Dynamic Model of Li-Ion Batteries Incorporating Electrothermal and Ageing Aspects for Electric Vehicle Applications, IEEE Transactions on Industrial Electronics 65 (2) (2018) 1298–1305. doi:10.1109/TIE.2017.2714118.
URL http://ieeexplore.ieee.org/document/7945538/

[2] X. Li, L. Zhang, Z. Wang, P. Dong, Remaining useful life prediction for lithium-ion batteries based on a hybrid model combining the long short-term memory and elman neural networks, Journal of Energy Storage 21 (2019) 510 – 518. doi:https://doi.org/10.1016/j.est.2018.12.011.
URL http://www.sciencedirect.com/science/article/pii/S2352152X1830450X

[3] T. Mesbahi, I.Jorge, T.Paul, S.Durand, Design and Simulation of Lithium-ion Battery Charger Using Forward Power Converter for Hybrid Energy Storage System, in: IEEE Vehicle Power and Propulsion Conference (VPPC'2019), 2019.

[4] G. K. Prasad, C. D. Rahn, Model based identification of aging parameters in lithium ion batteries, Journal of Power Sources 232 (2013) 79–85. doi:10.1016/j.jpowsour.2013.01.041.
URL http://linkinghub.elsevier.com/retrieve/pii/S0378775313000700

[5] A. Khaligh, Z. Li, Battery, ultracapacitor, fuel cell, and hybrid energy storage systems for electric, hybrid electric, fuel cell, and plug-in hybrid electric vehicles: State of the art, IEEE Transactions on Vehicular Technology 59 (6) (2010) 2806–2814.

[6] R. Xiong, Y. Zhang, J. Wang, H. He, S. Peng, M. Pecht, Lithium-Ion Battery Health Prognosis Based on a Real Battery Management System Used in Electric Vehicles, IEEE Transactions on Vehicular Technology 68 (5) (2019) 4110–4121. doi:10.1109/TVT.2018.2864688.

[7] T. Mesbahi, F. Khenfri, N. Rizoug, K. Chaaban, P. Bartholome?s, P. Le Moigne, Dynamical modeling of Li-ion batteries for electric vehicle applications based on hybrid Particle Swarm-Nelder-Mead (PSO-NM) optimization algorithm, Electric Power Systems Research 131 (2016). doi:10.1016/j.epsr.2015.10.018.

[8] P. Leijen, D. A. Steyn-Ross, N. Kularatna, Use of Effective Capacitance Variation as a Measure of State-of-Health in a Series-Connected Automotive Battery Pack, IEEE Transactions on Vehicular Technology 67 (3) (2018) 1961–1968. doi:10.1109/TVT.2017.2733002.

[9] D. Chen, J. Jiang, X. Li, Z. Wang, W. Zhang, Modeling of a pouch lithium ion battery using a distributed parameter equivalent circuit for internal non-uniformity analysis, Energies 9 (11) (2016). doi:10.3390/en9110865.

[10] D. Dvorak, H. Lacher, D. Simic, Thermal Modeling and Validation of a Lithium-Ion Battery Based on Electric Vehicle Measurements, 2014 IEEE Vehicle Power and Propulsion Conference (VPPC) (2014)

1–6doi:10.1109/VPPC.2014.7007144.
URL http://ieeexplore.ieee.org/lpdocs/epic03/wrapper.htm?arnumber=7007144

[11] C. Alaoui, Solid-State Thermal Management for Lithium-Ion EV Batteries, IEEE Transactions on Vehicular Technology 62 (1) (2013) 98–107. doi:10.1109/TVT.2012.2214246.
URL http://ieeexplore.ieee.org/document/6293912/

[12] C. Forgez, D. Vinh Do, G. Friedrich, M. Morcrette, C. Delacourt, Thermal modeling of a cylindrical LiFePO4/graphite lithium-ion battery, Journal of Power Sources 195 (9) (2010) 2961–2968. doi:10.1016/j.jpowsour.2009.10.105.

[13] N. Damay, C. Forgez, M. P. Bichat, G. Friedrich, A method for the fast estimation of a battery entropy-variation high-resolution curve – Application on a commercial LiFePO4/graphite cell, Journal of Power Sources 332 (2016) 149–153. doi:10.1016/j.jpowsour.2016.09.083.

[14] M. Fleckenstein, S. Fischer, O. Bohlen, B. Bäker, Thermal Impedance Spectroscopy - A method for the thermal characterization of high power battery cells, Journal of Power Sources 223 (2013) 259–267. doi:10.1016/j.jpowsour.2012.07.144.

[15] J. P. Schmidt, A. Weber, E. Ivers-Tiffée, A novel and precise measuring method for the entropy of lithium-ion cells: Δs via electrothermal impedance spectroscopy, Electrochimica Acta 137 (2014) 311–319. doi:10.1016/j.electacta.2014.05.153.

[16] S. Du, Y. Lai, L. Ai, L. Ai, Y. Cheng, Y. Tang, M. Jia, An investigation of irreversible heat generation in lithium ion batteries based on a thermo-electrochemical coupling method, Applied Thermal Engineering 121 (2017) 501–510. doi:10.1016/j.applthermaleng.2017.04.077.

[17] M. T. Lawder, P. W. Northrop, V. R. Subramanian, Model-based SEI layer growth and capacity fade analysis for EV and PHEV batteries and drive cycles, Journal of the Electrochemical Society 161 (14) (2014) A2099–A2108. doi:10.1149/2.1161412jes.

[18] A. Hentunen, T. Lehmuspelto, J. Suomela, Electrical battery model for dynamic simulations of hybrid electric vehicles, 2011 IEEE Vehicle Power and Propulsion Conference (2011) 1–6doi:10.1109/VPPC.2011.6043164.
URL http://ieeexplore.ieee.org/lpdocs/epic03/wrapper.htm?arnumber=6043164

[19] R. Sadoun, N. Rizoug, P. Bartholomeus, B. Barbedette, P. Le Moigne, Optimal sizing of hybrid supply for electric vehicle using Li-ion battery and supercapacitor, in: 2011 IEEE Vehicle Power and Propulsion Conference, IEEE, 2011, pp. 1–8. doi:10.1109/VPPC.2011.6043183.
URL http://ieeexplore.ieee.org/lpdocs/epic03/wrapper.htm?arnumber=6043183

[20] K. A. Severson, Attia, all., Data-driven prediction of battery cycle life before capacity degradation, Nature Energy 4 (5) (2019) 383–391. doi:10.1038/s41560-019-0356-8.
URL http://dx.doi.org/10.1038/s41560-019-0356-8